Nat Hazards (2014) 71:2143–2164
DOI 10.1007/s11069-013-1002-6

ORIGINAL PAPER

# Probability-based damage assessment for reinforced concrete bridge columns considering the corrosive and seismic hazards in Taiwan

**Chien-Kuo Chiu · Yue-Cong Lyu · Wen-Yu Jean**

Received: 23 September 2013 / Accepted: 10 December 2013 / Published online: 29 December 2013


**Abstract** In this paper, we consider the time at which earthquake events occur when analyzing seismic structural damage to a deteriorating RC bridge within a specified period. Because the uncertainty exists in the occurrence time of earthquake events, Monte Carlo simulation is applied. The proposed procedure for evaluating the exceedance probability, which corresponds to a specified limit state, is then applied to a case study of RC bridges in Taiwan to demonstrate its applicability. This study selects three typical RC bridges located in the Taipei Basin, Taiwan, to analyze exceedance probabilities of specified damage states during various specified periods and then discusses the cumulative damage effect on the exceedance probabilities of specified damage states. Additionally, for the chloride-induced deteriorating bridges at various distances to the sea in Suao, Taiwan, the effects of the deterioration and seismic structural damage on the exceedance probabilities of specified damage states are demonstrated and discussed. The proposed assessment procedure can help engineers understand whether the deterioration would accelerate the declining seismic performance of bridges and shorten their serviceability-related and safety-related service lives, as well as provide reference for repairing RC bridges and retrofitting their seismic performance.

**Keywords** Seismic structural damage · Cumulative damage · Chloride-induced corrosion · Reinforced concrete bridge

## 1 Introduction

Reinforced concrete (RC) structures typically deteriorate over time in corrosive environments. The deterioration of RC structures is the result of a reduction in structural capacity

C.-K. Chiu (✉) · Y.-C. Lyu
Department of Construction Engineering, National Taiwan University of Science and Technology, No. 43, Sec. 4, Keelung Rd., Taipei, Taiwan
e-mail: ckchiu@mail.ntust.edu.tw

W.-Y. Jean
National Center for Research on Earthquake Engineering, No. 200, Sec. 3, Xinhai Rd., Taipei, Taiwan

caused mainly by chloride ingress or carbonation, both of which usually lead to steel corrosion, loss of effective cross-sectional area of steel reinforcements, concrete cracking, loss of bonding between the reinforcing steel and concrete, and spalling of concrete cover. To maintain the structural safety and serviceability of such structures, maintenance strategies must be implemented. Moreover, corroded structural members, beams, or columns with reinforced steel components should be repaired once corrosion causes are identified. In recent years, life-cycle cost (LCC) modeling of these structures has garnered widespread attention and many researchers have developed methods that minimize LCCs as appropriate maintenance strategies. However, to identify appropriate life-cycle maintenance strategies for RC structures, one cannot overlook that fact that structural properties are time-dependent and typically decline due to corrosion within a structure's specified period.

While most studies assessing the LCCs of bridges have underscored the importance of maintenance and repair strategies (Kong and Frangopol 2003; Frangopol and Liu 2007), others have addressed the effects of extreme events on a structure's LCCs (Takahashi et al. 2004, 2006). Additionally, the economic cost-benefit ratio has been applied in decision analysis for seismically retrofitted structures. For instance, Williams et al. (2009) developed a method for making informed decisions about whether to retrofit structures for seismic events based on the expected economic benefits derived from retrofitting. To identify upfront costs and the long-term benefits of seismic retrofitting, Padgett et al. (2010) applied a risk-based method to assess seismic LCCs and the benefits of retrofitting bridges. However, only a few studies have developed life-cycle maintenance strategies for RC structures in corrosive environments with high seismic hazard. These strategies decrease the LCCs and losses induced by safety and serviceability failures occurring during earthquakes (Kumar et al. 2009; Chiu et al. 2008).

Compared to deterioration, which is generally slow and caused mainly by environmental factors, seismic structural damage is often manifested a sudden decline in structural capacity. Additionally, for an RC structure in a region with high seismic hazard, cumulative damage by deterioration and earthquakes markedly affects maintenance strategies. For instance, after an earthquake, an RC structure may have varying degrees of damage. When this damage is not repaired, the structure may be damaged further by subsequent earthquakes. Clearly, a structure is likely to sustain significant damage in an earthquake when it was damaged by a previous earthquake. The seismic structural damage over time has also been widely discussed and studied via LCC modeling. The accumulation of seismic structural damage over time has also been widely discussed and studied via modeling of LCCs. For instance, Sanchez-Silva et al. (2011) presented a developed stochastic model to characterize the sudden degradation of structural performance due to short-term or sudden events (e.g., earthquakes, terrorist attacks, or accidents) and progressive deterioration (e.g., biodegradation, sulfur attack, corrosion, and fatigue). Although Sanchez-Silva et al. (2011) assumed degradation does not depend on existing damage states in the research, their model can propose analytical solutions for the degradation of structural performance induced by short-term or sudden events and progressive deterioration. Additionally, because analytical solutions for damage-dependent degradation of structural performance are difficult to derive, an assessment procedure is needed that considers cumulative damage caused by deterioration and earthquakes simultaneously when estimating structural performance.

In Taiwan, many steel and RC structures near the coast have chloride-induced damage (Fig. 1). As the service period of structures increases, their safety and serviceability decrease. Restated, the original designed service life and safety reliability depreciate when structures are adversely affected by environmental factors such as chloride concentration

**Fig. 1** Chloride-induced corrosion in an RC bridge

and carbonation. However, because earthquakes are common in Taiwan, repairing or retrofitting structures is mainly based on their seismic performance. Unless corrosion reduces the structural safety of a structure, "pre-damage" maintenance work is seldom applied to prevent the serviceability from being reduced by corrosion. Therefore, in structural design, unlike cases that are usually analyzed (e.g., probabilistic seismic hazard analysis), research is lacking in Taiwan that assesses the environmental hazard in a marine environment. Restated, engineers require a model that can quantify accurately corrosion hazard induced by the marine environment.

This work considers the time at which earthquake events occur when analyzing seismic structural damage to a deteriorating RC bridge within a specified period. Because uncertainty exists in predicting the time at which an earthquake will occur, Monte Carlo simulation (MCS) is applied. The proposed procedure for evaluating exceedance probability, which corresponds to a specified limit state, is then applied to a case study of RC bridges in Taiwan to demonstrate its applicability. This work selects three typical RC bridges in the Taipei Basin, Taiwan, to analyze exceedance probabilities of specified damage states during various specified periods and then discusses the cumulative damage effect on exceedance probabilities of specified damage states. Additionally, as these chloride-induced deteriorating bridges are at various distances to the sea in Suao, Taiwan, the effects of deterioration and seismic structural damage on exceedance probabilities of specified damage states are demonstrated and discussed. The proposed assessment procedure will allow engineers to determine whether deterioration will accelerate the declining in seismic performance of a bridge and shorten its serviceability- and safety-related service lives, as well as provide reference for repairing an RC bridge and retrofitting its seismic performance.

## 2 Chloride-induced corrosive environment

In order to quantify the hazard of corrosion induced by chloride, this study acquires data of chloride deposits and corrosion rates of carbon steel exposed to air from test points along

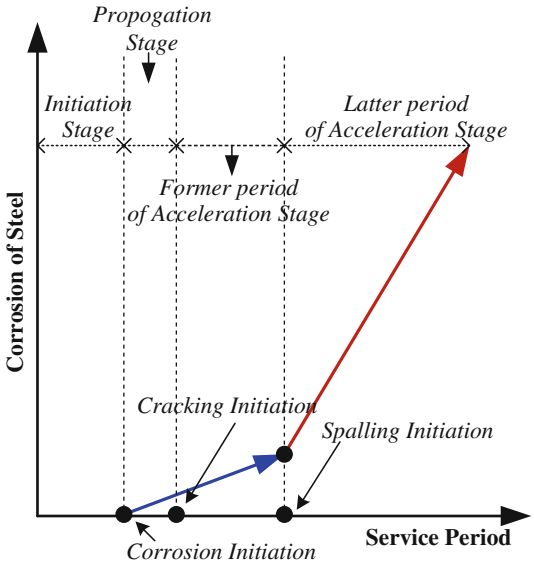


**Fig. 2** Deterioration process induced by chloride ingress

the measurement lines from Taiwan's Harbor and Marine Technology Center. To predict the corrosion-induced weight loss of reinforcing steel bars (Tottori and Miyagawa 2004), besides the corrosion rate (propagation and acceleration stages), the time required for chloride to corrode reinforcing steel bars (initiation stage) must be simulated using equations that estimate the air-borne chloride concentration, the chloride concentration on concrete surfaces, and the diffusion of chloride ions. Figures 2 and 3 show the corrosion process induced by chloride and the calculation procedure for the weight loss of reinforcement induced by chloride, respectively.

## 2.1 Air-borne chloride concentration in Taiwan's coastal regions

Ministry of transportation and communications in Taiwan inspected 203 bridges in 2002 to identify and analyze chloride environments in coastal regions (MOTC 2010a, 2011). Inspection results indicated that the amount of chloride adhering to the bridges decreased as distance between a bridge and the coastline increased. Moreover, when a structure and the coastline are separated by a distanced exceeding 3 km, the amount of chloride adhering to concrete surfaces is very low; therefore, the impact of chloride ions on steel structures or RC structures can generally be ignored. That is, the distance used by Ministry of transportation and communications in Taiwan during its investigations of chloride-induced corrosion was 3 km from the coastline. Test points for chloride deposits were arranged along inland lines, which run vertical to the coastline. Test points in each measurement line were set at 100, 300 m, 1, and 3 km from the coastline (Fig. 4). Moreover, collectors of chloride deposits use the wet-candle method (CNS 13754 1996), which exposes wet fibers to air in a given area for a set duration; a chemical analysis is then conducted to measure the deposits ($mg/m^2/day$). This work acquired data from test points along measurement lines from Taiwan's Harbor and Marine Technology Center. These data are for chloride deposits and corrosion rates of carbon steel exposed to air (CNS 13753 2005) between August 2009 and December 2010 (MOTC 2010a, 2011).

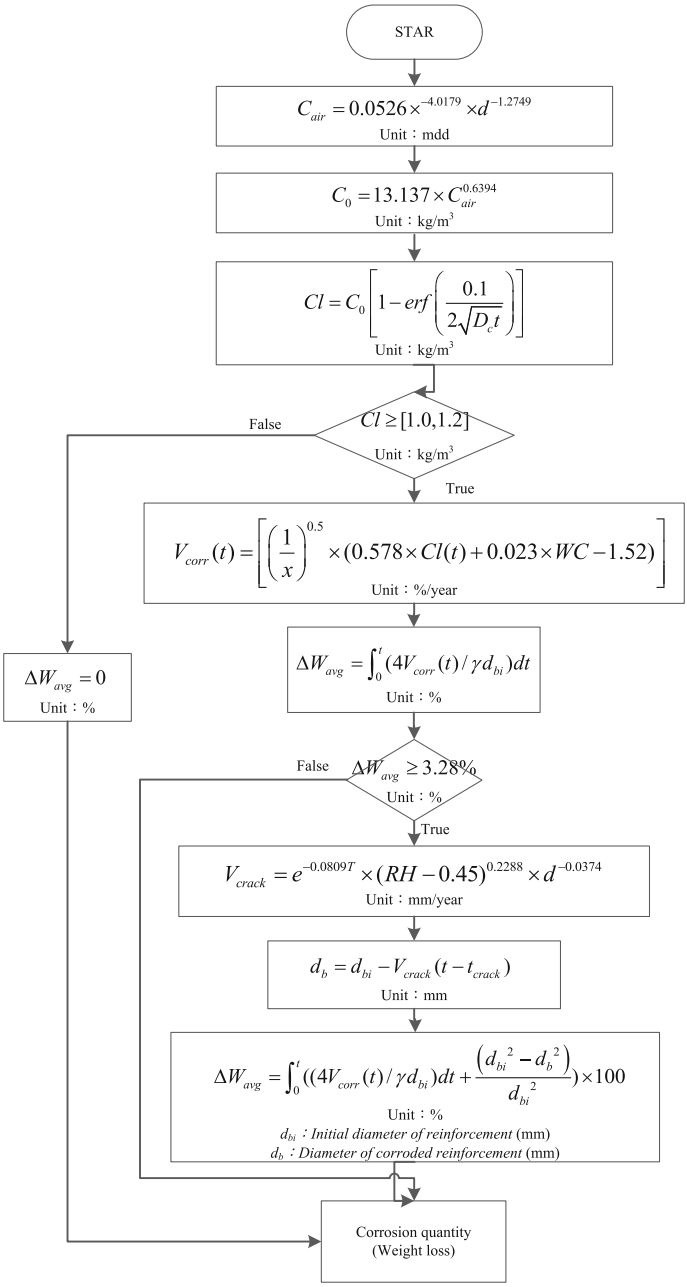


**Fig. 3** Calculation procedure for the weight loss of reinforcement induced by chloride ingress

This work applies the estimation equation established by JSCE (JSCE 2008) for estimating air-borne chloride concentrations $C_{\text{air}}$ and considers influential parameters, including the ratio of sea wind $r$ (defined as the percentage of time during 1 day when the wind is blowing from sea toward load), mean wind speed $u$, and distance to the nearest

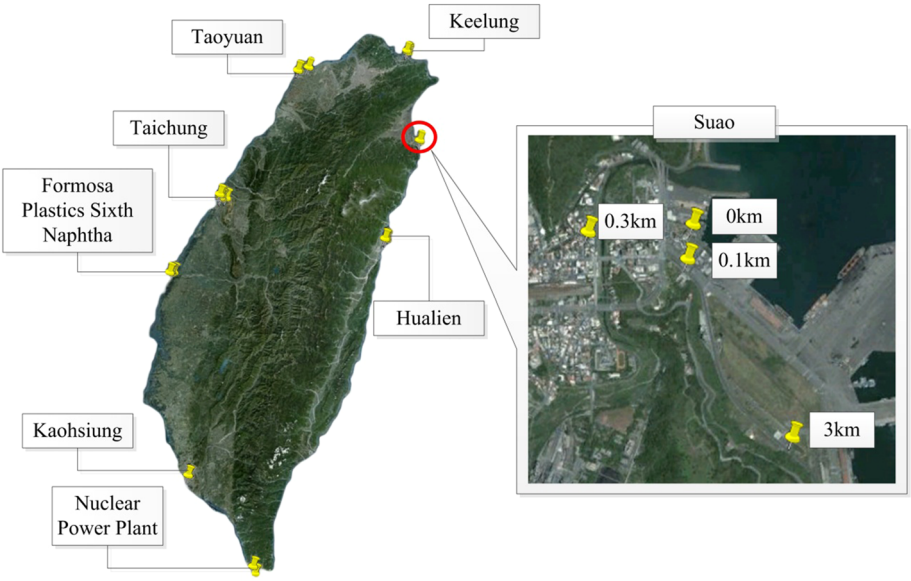


**Fig. 4** Test points for chloride deposits in each measurement line in Taiwan

**Table 1** Regression equations for air-borne chloride concentration

| Measurement line | Air-borne chloride concentration | Mean value of model error[a] | COV of model error[a] |
|---|---|---|---|
| Taoyuan | $C_{air} = 0.46 \times u^{-3.97} \times d^{-1.91}$ | 1.47 | 0.75 |
| Suao | $C_{air} = 0.05 \times u^{-4.02} \times d^{-1.27}$ | 2.56 | 0.90 |
| Taichung | $C_{air} = 0.16 \times u^{-5.53} \times d^{-0.92}$ | 3.30 | 0.55 |
| Hualien | $C_{air} = 0.10 \times u^{-2.53} \times d^{-1.31}$ | 2.88 | 0.71 |
| Kaohsiung | $C_{air} = 0.05 \times u^{-2.92} \times d^{-1.05}$ | 4.42 | 0.58 |

[a] $C_{air}$ is the air-borne chloride concentration (mdd); $r$ is the ratio of sea wind ratio; $u$ is mean wind speed (m/s); and $d$ is distance to the nearest coastline (km). Model error = measured data/regression data

coastline $d$ to develop the equations for estimating air-borne chloride concentrations in Taiwan's coastal regions, as shown in Eq. (1). The data for wind speed, including its mean value and standard deviation, were obtained from the Web site maintained by Central Weather Bureau of Taiwan (http://www.cwb.gov.tw). Table 1 shows the regression equations of measurement lines, including the model error with the mean value and coefficient of variation for each regression equation.

$$C_{air} = 1.29 \times r \times u^{0.386} \times d^{-0.952} \quad (1)$$

## 2.2 Chloride-induced corrosion process

For chloride-induced corrosion in Taiwan's coastal regions, based on mean wind speed and distance to the nearest coastline, the air-borne chloride concentration, $C_{air}$, is determined

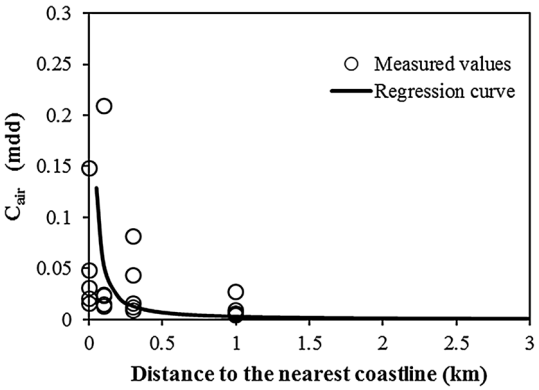


**Fig. 5** Regression equation for air-borne chloride concentration in Suao

using the regression equations. Figure 5 shows measured values and regression results in Suao of Taiwan. Table 1 shows the regression equations of measurement lines, including the model error with the mean value and coefficient of variation for each regression equation. Because not all chloride deposits remain on concrete surfaces, air-borne chloride concentrations should be modified to include the chloride concentrations on concrete surfaces, which are needed in a diffusion simulation of chloride ions in concrete. Therefore, this paper uses data for the chloride concentration on concrete surfaces investigated in the past research (Chen and Chan 2010) and the equations for estimating air-borne chloride concentrations stated above to find the relationship between the chloride deposits and chloride concentrations on concrete surfaces, as shown in Eq. (2).

Fick's second law can then be applied to estimate the time when chloride ions diffuse from concrete surfaces to a passive film on the surface of reinforcing steel bars,

$$C_o = 13.14 \times C_{\text{air}}^{0.64} \tag{2}$$

$$\text{Cl} = C_o\left[1 - \text{erf}\left(\frac{0.1 \times c}{2\sqrt{D_c t}}\right)\right] \tag{3}$$

$$\log D_c = -6.77(\text{w/c})^2 + 10.1(\text{w/c}) - 3.14 \tag{4}$$

where Cl is the chloride concentration on the surface of reinforcing steel bars (kg/m$^3$); $C_o$ is the chloride concentration of the concrete surface (kg/m$^3$); $c$ is diffusion distance, which is the thickness of the concrete cover (mm); $D_c$ is the apparent diffusion coefficient of chloride ions (cm$^2$/year); w/c is the water–cement ratio; $t$ is a specified service period (year); and erf is the error function.

Based on the observation results obtained by Kato and Uomoto (2005), we assume corrosion initiates when the chloride concentration on the surface of reinforcing steel bars reaches a threshold, which is a random variable distributed uniformly in the range of 1.0–1.2 kg/m$^3$. This paper accounts for uncertainties in chloride-induced deterioration analysis of this stage that are related to the apparent diffusion coefficient, concrete cover thickness, and the chloride concentration on concrete surfaces caused by the environmental and construction conditions (JSCE 2008). The corrosion probability can be calculated using MCS; then, 10 % (ASTM C876 1991) is set as a threshold to determine the corrosion initiation on them.

Based on an existing deterioration model (Takahashi et al. 2005), we assume that the rate of corrosion (mg/cm$^2$/year) in the propagation stage is treated as a lognormal random

variable with a mean value, which can be derived using Eq. (5), and a coefficient of variation of 0.5. The effect of corrosion on material degradation is assessed according to the degree of corrosion of reinforcing steel bars, where weight loss is typically used as a quantifiable measure, as in Eq. (6).

$$V_{\text{corr}} = \frac{78}{\sqrt{c}}(0.578 \times \text{Cl} + 0.023(\text{w/c}) - 1.52) \tag{5}$$

$$\Delta W_{\text{avg}} = \frac{4V_{\text{corr}}}{\gamma \times d_i} \tag{6}$$

where $\gamma$ is the density of reinforcing steel bars (mg/cm$^3$; approximately 7850), and $d_{bi}$ is the diameter of reinforcing steel bars (mm).

Most studies used experimental field-exposure results to determine the relationship between degree of corrosion of reinforcing steel bars and occurrence of corrosion-induced cracking. Additionally, according to Tottori and Miyagawa (2004), we assume that the corrosion rate in the propagation stage and former period of acceleration stage is the same.

According to the Architecture Institute of Japan (AIJ; AIJ 1997), spalling of a concrete cover is caused by the formation of cracks with widths exceeding 0.5–1.0 mm. The corresponding initiation threshold of the latter period of acceleration stage is difficult to define. In this paper, the empirical result obtained by Izawa and Matusima (2004) is used to set the threshold as the weight loss percentage of corroded reinforcing steel of 3.28 %, which is treated as a lognormal distribution with 0.26 as the coefficient of variation. Additionally, one can reasonably assume that the concrete surface spalls severely, such that the concrete cover cannot prevent reinforcing steel bars from corroding in the latter period of acceleration stage.

Although the corrosion rate can be set as the corrosion rate of reinforcing steel bars unprotected by concrete, only few studies have discussed corrosion of reinforcing steel bars resulting from concrete cover spalling (Tottori and Miyagawa 2004). To consider the effects of environmental conditions on the corrosion rate of reinforcing steel bars, this paper uses data for the corrosion rate of carbon steel exposed to air at all test points along measurement lines on the basis of the references (Niu 2003; Sung et al. 2010).

### 2.3 Corrosion rate of carbon steel exposed to air in Taiwan's coastal regions

Based on the research conducted by Niu (2003), four important factors are sensitive to the corrosion rate of reinforcing steel embedded in concrete, $V_{\text{crack}}$: temperature, $T$ (°C), humidity, RH (%), concrete cover thickness, $c$ (mm), and time, $t$ (year), as Eq. (7).

$$V_{\text{crack}} = \alpha \times \exp(\beta \times T)\left(\frac{\text{RH}}{100} - 0.45\right)^{\kappa} c^{-\lambda} t^{\eta} \tag{7}$$

where $\alpha$, $\beta$, $\kappa$, $\lambda$, and $\eta$ are the five coefficients to be determined.

Based on the corrosion rate of carbon steel exposed to air at test points along measurement lines (MOTC 2010a, 2011) and data for temperature and humidity from Central Weather Bureau of Taiwan, the equations for estimating corrosion rate in Taiwan's coastal regions were regressed (Table 2). Referring to the above deterioration model for chloride-induced corrosion, corrosion curves of reinforcing steel bars, which show the relationship between mean weight loss and time, can be plotted to estimate degradation of the material properties of reinforcing steel bars (e.g., yielding strength, elasticity modulus, and ultimate strength). Additionally, these degradation curves of the material properties of reinforcing

**Table 2** Regression equations for the corrosion rate of carbon steel for the coastal regions in Taiwan

| Division zone | Measurement line | $V_{crack}$ (mm/year) | Mean value of model error | COV of model error |
|---|---|---|---|---|
| Northern | Suao | $V_{crack} = e^{-0.08T} \times \left(\frac{RH}{100} - 0.45\right)^{0.23} \times d^{-0.04}$ | 1.13 | 0.58 |
| Middle | Taichung | $V_{crack} = e^{-0.05T} \times \left(\frac{RH}{100} - 0.45\right)^{0.94} \times d^{-0.05}$ | 1.31 | 0.73 |
| Southern | Kaohsiung | $V_{crack} = e^{-0.02T} \times \left(\frac{RH}{100} - 0.45\right)^{1.77} \times d^{-0.06}$ | 1.03 | 0.50 |
| Eastern | Hualien | $V_{crack} = e^{-0.09T} \times \left(\frac{RH}{100} - 0.45\right)^{0.28} \times d^{-0.09}$ | 0.92 | 0.30 |

T: mean value of temperature (°C), RH: mean value of humidity (%)

steel bars are needed in the assessment of the time-dependent seismic performance or structural properties for a chloride-induced deteriorating RC bridge (MOTC 2010b).

## 3 Life-cycle earthquake simulation

### 3.1 Seismic hazard analysis

To identify ground motion during an earthquake, Taiwan's Central Weather Bureau implemented the Taiwan Strong Motion Instrumentation Program (TSMIP) in 1990. About 700 free-field accelerometers have been established in metropolitan areas that have large concentrated populations. These accelerometers, which are located near faults and in different geologic environments, record complete earthquake data to structure the empirical method for site effect analysis.

Research by Jean et al. (2002) used these earthquake data to construct a prediction model of earthquake intensity that considers the effects on various sites and then generated a site correction function, as in Eqs. (9) and (10). Equation (9) is the attenuation law of ground acceleration, $Y_a$, and Eq. (10) is the site correction function for $Y_a$. The Taipei Basin has unique geologic and topographic effects from seismic waves that cannot be reflected by simple site classification or basement depth. According to earthquake records, the intensity attenuation law was analyzed in two steps: First, the earthquake intensity prediction model meeting the site effect was built; and second, the special site effect of the Taipei Basin was analyzed according to the records of several major earthquakes in recent years. For the Taipei Basin, far-field earthquakes are divided into regional and fault earthquakes: Regional earthquakes were in Yilan (ZS01) and Hualien (ZS02), as shown in Fig. 6, while fault earthquakes were on the Hsincheng, Tuntzuchiao, and Milun faults (NCREE 2005). Additionally, to address the effect of far-field earthquakes on the Taipei Basin, time-history data for the 921 Jiji Earthquake, which were recorded by stations TAP013 (Tapei Zone I), TAP022 (Taipei Zone II), and TAP088 (Taipei Zone III), are modified such that they are compatible with the code-required response spectrum of acceleration for a specified site and are used for simulation in the case study.

$$Y_a = b_1 \exp(b_2 M)[R + b_4 \exp(b_5 M_L)]^{-b_3} \tag{9}$$

$$\ln(Y_0) = C_1 + C_2 \times \ln(Y_a) \tag{10}$$

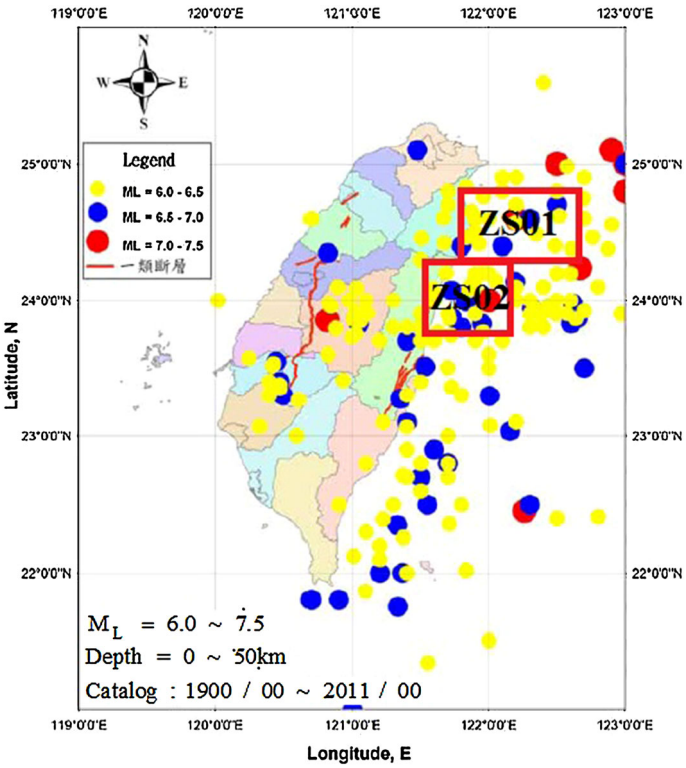


**Fig. 6** Regional earthquakes of ZS01 (Yilan) and ZS02 (Hualien) (NCREE 2005)

where $b_1$, $b_2$, $b_3$, $b_4$, $b_5$, $C_1$, and $C_2$ are constants, which can be obtained using regression analysis; $R$ is the distance between an earthquake's epicenter and structure's site (km); and $Y_a$ and $Y_0$ are the ground accelerations (g).

### 3.2 Life-cycle earthquake events induced by a specified hypocenter

Generally, to calculate cumulative damage due to earthquake events at a specified hypocenter, one must know the number of events and their magnitudes that will likely occur within a given time window. Let the seismicity of a contributing hypocenter be known a priori in terms of occurrence rates of earthquakes of different magnitudes. Further, let the average rate of occurrence/year, $N$, of earthquakes of magnitude $\geq M_L$ at a specified hypocenter be described by the Gutenberg–Richter relationship (G–R curve) as

$$\log N = a - b \times M_L \tag{11}$$

where $a$ and $b$ are constants estimated from the catalog of past earthquakes or from the known slip rate at a specified hypocenter. Figure 7 shows the G–R curves for the hypocenters ZS01 and ZS02.

When we assume all events of magnitude $\geq M_L$ at a hypocenter follow a Poisson sequence of occurrences, $1/N$ represents the mean return period of occurrence of those events. Notably, due to its lack of memory, the Poisson process cannot accommodate

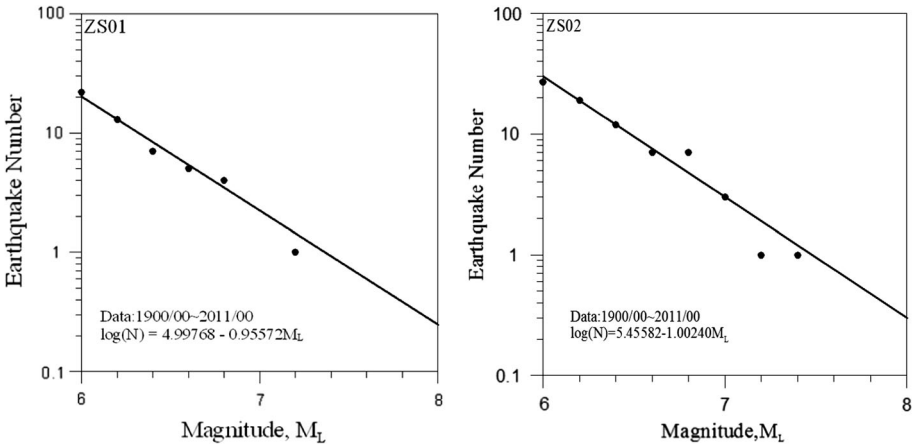


**Fig. 7** G–R curves of ZS01 and ZS02

effectively large magnitudes. To simulate large earthquakes, many recent models assumed a lognormal or Weibull distribution of return periods, whose hazard functions are time-dependent. The number of occurrences within a given period depends on knowledge of occurrence time of the previous event. These models represent accurately the occurrences of large earthquakes in many regions. However, in addition to providing statistical evidence to support seismic gap and a typical earthquake hypothesis, engineers frequently have trouble in using simulation models that have lognormal or Weibull distributions for return periods to estimate the number of earthquakes that will occur. In this work, because the Poisson process is not physically unreasonable for small-to-medium events of, it can be used when simulating the occurrence times of earthquakes within a specified period, facilitating the study of the cumulative damage effect. Notably, aftershocks are not addressed in this work.

If $f(t)$ is the probability density function of the return period and $F(t)$ is the corresponding cumulative probability distribution, the hazard rate is the number of events in the time interval $(t, t + dt)$, as in Eq. (12). Additionally, Eq. (13) can estimate the expected number of events that will occur in a specified period $T$. When earthquake occurrence has Poisson distribution, the return period has exponential distribution, and the hazard rate then is constant (irrespective of quiescent period duration) and equal to the number of occurrences per unit time.

$$h(t) = \frac{f(t)}{1 - F(t)} \tag{12}$$

$$\bar{N}(T_o + T|T_o) = \int_{T_o}^{T_o+T} h(\tau)\mathrm{d}\tau \tag{13}$$

Once the number of earthquakes is predicted for a hypocenter, the maximum magnitude during a given number of years can be estimated for a confidence level by extreme-event analysis. However, no methodology exists to estimate the magnitudes of the second largest and higher-order events. Therefore, we assume that events likely occurring at a hypocenter over a given period are statistically independent and the order statistics approach estimates

the magnitudes of ordered events (Das et al. 2007). The expected magnitude of the $i$th largest event is thus estimated as

$$E\left[M_L^i\right] = \int_{M_L^{\min}}^{M_L^{\max}} m p_i(m) \mathrm{d}m \tag{14}$$

$$p_i(m) = \frac{\bar{N}!}{(\bar{N}-i)!(i-1)!}[F(m)]^{i-1}[1-F(m)]^{\bar{N}-i}p(m) \tag{15}$$

where $p_i(m)$ is the probability density function of the $i$th largest event. In Eq. (15), $\bar{N}$ is the expected number of events in $T$ years in the range $\left[M_L^{\min}, M_L^{\max}\right]$, which are the maximum and minimum magnitudes observed in the past earthquake record, respectively, and $F(m)$ and $p(m)$ are, respectively, the probability distribution and density functions of $\bar{N}$ events in models with time-dependent hazard rates. Here, $\bar{N}(m)$ is the expected number of events in $T$ years the range $\left[m, M_L^{\max}\right]$; and $p(m)$ is evaluated numerically via the finite-difference method. For the model with constant hazard rate, the number of earthquakes over the entire magnitude range is estimated from the G–R curve, and thus, $p(m)$ and $F(m)$, respectively, are derived as

$$p(m) = b \ln 10 \frac{10^{-b\left(m-M_L^{\min}\right)}}{1-10^{-b\left(M_L^{\max}-M_L^{\min}\right)}} \tag{16}$$

$$F(m) = \frac{10^{-b\left(m-M_L^{\min}\right)} - 10^{-b\left(M_L^{\max}-M_L^{\min}\right)}}{1-10^{-b\left(M_L^{\max}-M_L^{\min}\right)}} \tag{17}$$

When the predicted number of earthquakes within a specified period is known, the times at which these earthquakes occur during this period can be modeled using random simulation, which we assume has a uniform distribution. Additionally, in this work, the intensity attenuation law (Sect. 3.1) was utilized to derive the peak ground acceleration of each earthquake for a specified site. For instance, Fig. 8 shows the predicted ordered earthquake events with a specified period of 100 years for the Taipei Zone I (TAP013) induced by the hypocenters ZS01 and ZS02.

## 4 Probability-based damage assessment for RC bridges

Uncertainty related to earthquakes or ground motion must be considered when assessing the possible seismic damage to a structure. This section applies a simulation procedure that obtains the exceedance probability curve, as it relates to a specified acceptable damage state for RC bridges in seismically active zones. Based on this exceedance probability curve, an engineer can identify the effect of cumulative damage associated with deterioration and earthquakes. Restated, simulated service life data can improve rational resource allocation and asset management.

### 4.1 Seismic damage index for RC bridges

The model developed by Park and Ang (1985), the most widely used in the literature (Cosenza et al. 2009), is a linear combination of maximum deformation response and hysteretic energy. The damage index of this model is expressed as

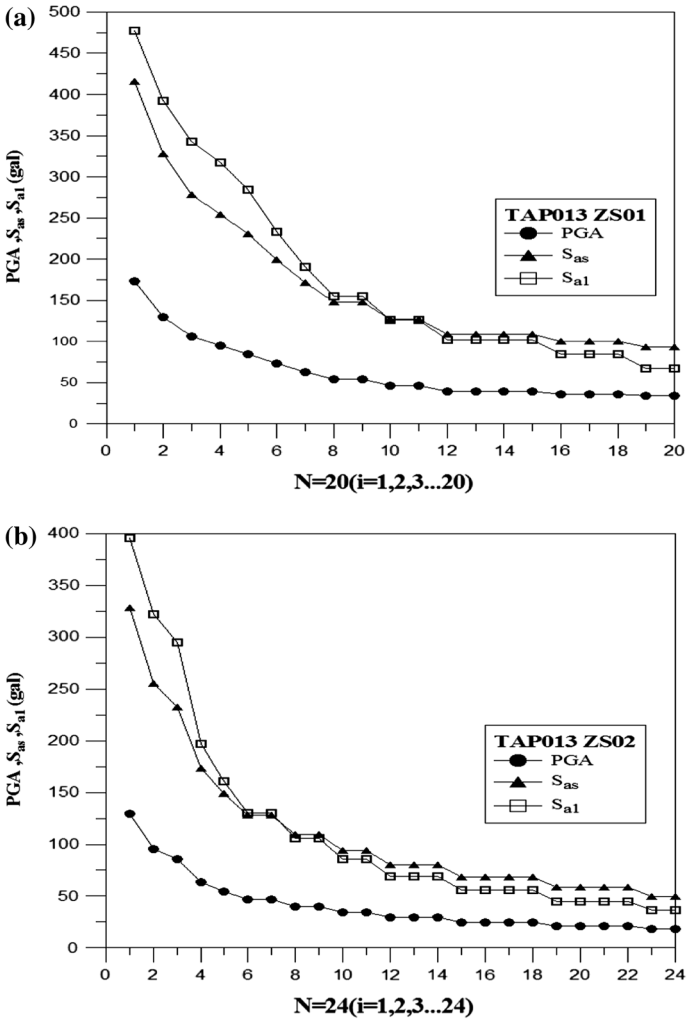


**Fig. 8** Predicted ordered earthquake events within a specified period of 100 years for the Taipei Zone I. **a** Hypocenter Z01 (Yilan), **b** hypocenter Z02 (Hualien)

$$D_{P\&A} = \frac{\delta_M}{\delta_u} + \frac{\beta \int \mathrm{d}E}{F_y \delta_u} \tag{18}$$

where $D_{P\&A}$ is the damage index—an empirical measure of damage ($D_{P\&A} \geq 1.0$ indicates total damage or collapse); $\delta_M$ is maximum response deformation; $\delta_u$ is ultimate deformation capacity under static loading; $F_y$ is calculated yielding strength; d$E$ is incremental absorbed hysteretic energy (excluding potential energy); and $\beta$ is the coefficient for cyclical loading effects (as a function of structural parameters, it can be set at 0.05 for general RC structures).

**Table 3** Classification of damage states for RC bridges

| Damage state | Damage index | Description |
|---|---|---|
| Non-damage | <0.1 | Slight cracks in nonstructural components |
| Slight damage | 0.1–0.2 | Slight cracks in structural components |
| Moderate damage | 0.2–0.4 | Flexure shear cracks in the top or bottom ends of piers. Spalling of the concrete cover. Shear cracks in the middle part of piers connected to windowsills. Obvious damage in nonstructural components. Loosening of stirrups in the top or bottom ends of piers |
| Serious damage | 0.4–1.0 | Crushed concrete in pier cores. Extensive loosing of stirrups. Buckling of main bars |
| Total damage or collapse | >1.0 | Extensive damage to piers. Extensive crushing of core concrete in piers and piers without any loading capacity. Partial or total bridge collapse, or close to collapse |

Previous experimental data and investigation information for classifying seismic structural damage states can be applied to set the $D_{P\&A}$ limiting value for each damage state; for instance, the limiting values of $D_{P\&A}$ for RC bridges (Table 3) were based on investigation data of the earthquake disaster (Suzuki et al. 1998) adopted in the case study herein. In this work, to reduce computing time when assessing the damage to an RC bridge, the single-degree-of-freedom (SDOF) system of an RC bridge estimates the structural damage corresponding to an earthquake event (Table 3). Nonlinear dynamic analysis is needed to estimate the maximum deformation response and hysteretic energy corresponding to an earthquake event. Additionally, to describe the hysteretic behavior of the one-component model in nonlinear dynamic analysis, a hysteretic law is needed. Since this work focuses on a relatively simple approach that can be used conveniently to investigate the seismic structural damage on RC bridges, the Takeda model (Takeda et al. 1972) was applied for nonlinear dynamic analysis of the maximum deformation response and hysteretic energy corresponding to an earthquake event for the SDOF system of an RC bridge (Fig. 9). Notably, the unloading stiffness of the adopted model is reduced by an exponential function of the previous maximum deformation response ($\alpha$ is the parameter of unloading degrading stiffness, and it was set at $-0.5$ in the case study; $\eta$ is the ratio between the stiffness after yielding and initial stiffness, and it was set at 0.001 in the case study).

In this work, pushover analysis is applied to simulate the capacity curve of a bridge, which is the relationship between base shear force and bridge deck displacement. The capacity curve is converted to the capacity spectrum, which represents structural performance of the SDOF system for a bridge. This conversion is accomplished by identifying the dynamic characteristics of a structure in terms of its first modal participation factor and its first modal mass coefficient. Further, this work utilizes the capacity spectrum in ATC-40 (ATC 1996) to determine ultimate deformation capacity, $\delta_u$, yielding strength, $F_y$, and the elastic fundamental period, $T_y$, of the SDOF system for a structure.

### 4.2 Modeling of cumulative structural damage incurred by earthquakes

An RC bridge will not be repaired when the seismic damage index is lower than a specified value corresponding to the damage state of "Without any damage"; therefore, it is necessary to modify the structural properties of the bridge on the basis of the residual and

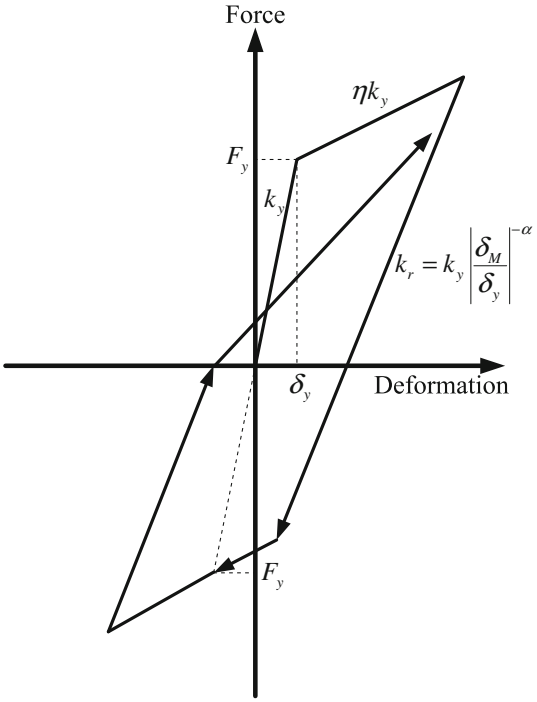


**Fig. 9** Takeda model for the nonlinear dynamic analysis

maximum deformation response for estimating the damage index corresponding to the next earthquake (Chiu et al. 2013). For instance, if an RC bridge is not repaired after the $(i-1)$th earthquake event, not only the dynamic response corresponding to the $(i-1)$th earthquake event but also the modification of the structural properties is considered in the estimation of the damage index corresponding to the next earthquake event $i$. In the modification of the structural properties (Fig. 10), except for the yielding base shear fore, which was assumed constant herein, the elastic fundamental period, ultimate deformation capacity, and yielding deformation need to be recalculated based on the maximum deformation response, $\delta_M^{i-1}$, and residual deformation, $\delta_r^{i-1}$, incurred by the $(i-1)$th earthquake event, as shown in Fig. 10. In this work, after the $(i-1)$th earthquake event, the ultimate deformation capacity, $\delta_u^i$, and yielding deformation, $\delta_y^i$, are assumed same as $\left(\delta_u^{i-1} - \left|\delta_r^{i-1}\right|\right)$ and $\left(\delta_M^{i-1} - \left|\delta_r^{i-1}\right|\right)$, respectively. For an RC bridge without any repair or retrofit, when the bridge is attacked by several earthquake events (the number of earthquake events is assumed to be $i$ in Eq. (19)) in a specified period, its seismic damage index after the $i$th event including the cumulative damage effect can be estimated using Eq. (19).

$$D_{P\&A}^i = \frac{\max\left\{\delta_1^{\mathrm{M}}, \delta_2^{\mathrm{M}}, \ldots, \delta_{\mathrm{i}}^{\mathrm{M}}\right\}}{\delta_u} + \frac{\beta}{F_y \delta_u} \sum_{i=1}^{i} \mathrm{d}E \tag{19}$$

### 4.3 Probability-based damage assessment for RC bridges

The proposed procedure for estimating the seismic structural damage of an RC bridge uses the MCS to consider uncertainties associated with earthquake events as stated in

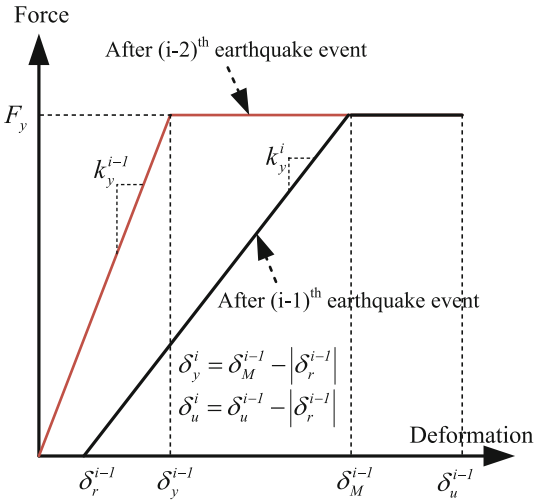


**Fig. 10** Modification of the structural properties in terms of the seismic structural damage

Sect. 3. In one calculation in the MCS, the seismic damage index corresponding to each earthquake event can be estimated using Eqs. (18) and (19), while considering the occurrence time and PGAs of earthquakes for a bridge within a specified period; then, the time-dependent seismic damage index within the specified period can be obtained. By means of incorporating the uncertainty in the occurrence of earthquake events in a specified period, the exceedance probability of a specified damage state can be estimated using the MCS.

Because the user or owner of a structure is very concerned about whether the structure would collapse or not due to earthquakes during its service life, this work focused on the exceedance probabilities corresponding to the states of "Serious damage" and "Moderate damage." This information can also help engineers to arrange maintenance plans.

## 5 Case study

Three RC bridges (Fig. 11) in Taiwan were selected to investigate the effect of sequential earthquakes and chloride-induced deterioration on their structural performance. Table 4 lists their structural properties. The SDOF parameters and structural performance of each RC bridge were taken from the specified performance points (Sect. 4.1; Table 4). Additionally, these parameters are needed to estimate the seismic damage index under sequential earthquakes. On the basis of the assessment procedure stated in Sect. 4.3, the simulation results and discussions are described as follows:

### 5.1 Taipei city as an example: RC bridges without deterioration

Figure 12 shows simulation results for exceedance probabilities of the specified damage states for the RC bridges. Figure 12a shows exceedance probabilities of moderate and severe damage states for Bridge-A (named by PE2 and PE3 in the figure, respectively), which is set at various zones in Taipei, by considering hypocenters ZS01 (Yilan) and ZS02 (Hualien). Obviously, Taipei Zone II (the time history of the 921 Jiji Earthquake recorded

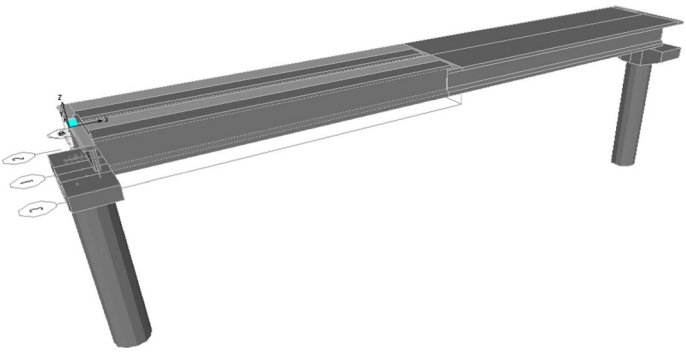

**Fig. 11** Structural model of the Bridge-A (2010b)

**Table 4** Structural properties of the selected RC bridges

| Properties | Bridge-A | Bridge-B | Bridge-C |
|---|---|---|---|
| Length (m) | 7@36.6 = 256 | 12@30 = 360 | 4@30 = 120 |
| Height (cm) | 1,080 | 800 | 600 |
| Diameter of pier (cm) | 180 | 200 | 300 |
| Spacing of stirrups (cm) | 20 | 15 | 20 |
| Number of main bars | 30 (#10) | 54 (#10) | 84 (#9) |
| $F_y$ (tf) | 90 | 449 | 473 |
| $\delta_y$ (cm) | 3.3 | 3.3 | 0.4 |
| $\delta_p$ (cm) | 11.3 | 7.9 | 1.0 |
| $S_{ay}$ (g) | 0.26 | 0.30 | 0.34 |
| $T_y$ (s) | 0.73 | 0.64 | 0.23 |

by station TAP022 is modified to be compatible with the code-required response spectrum of acceleration and is applied for nonlinear dynamic analysis) would incur greater seismic damage than other locations in ZS01 and ZS02; Bridge-B and Bridge-C have similar findings. Except for Taipei Zone II and Zone III, the exceedance probabilities of the serious damage state are zero regardless of selected bridge and hypocenter (Fig. 12). Therefore, the effect of cumulative seismic damage can be neglected in simulation of exceedance probability of the serious damage for Taipei Zone I.

In this work, the seismic damage index defines the limit state function. Restated, the damage index for an earthquake and its limiting value (Table 3) are considered "structural response" and "acceptable limit for structural response," respectively. For serviceability-related service life, moderate damage is considered an acceptable limit for structural response. Additionally, serious damage is utilized to define service life for bridge safety. For the selected RC bridges, when the acceptable value of reliability is set at 0.50, safety-related service lives are 20 (Bridge-A), 23 (Bridge-B), and 35 (Bridge-C) years when considering hypocenter ZS02; for hypocenter ZS01, their safety-related service lives equal to almost 10 years. Based on the concept of preventive maintenance, the acceptable value of reliability related to serviceability is set at 0.50; therefore, the corresponding service

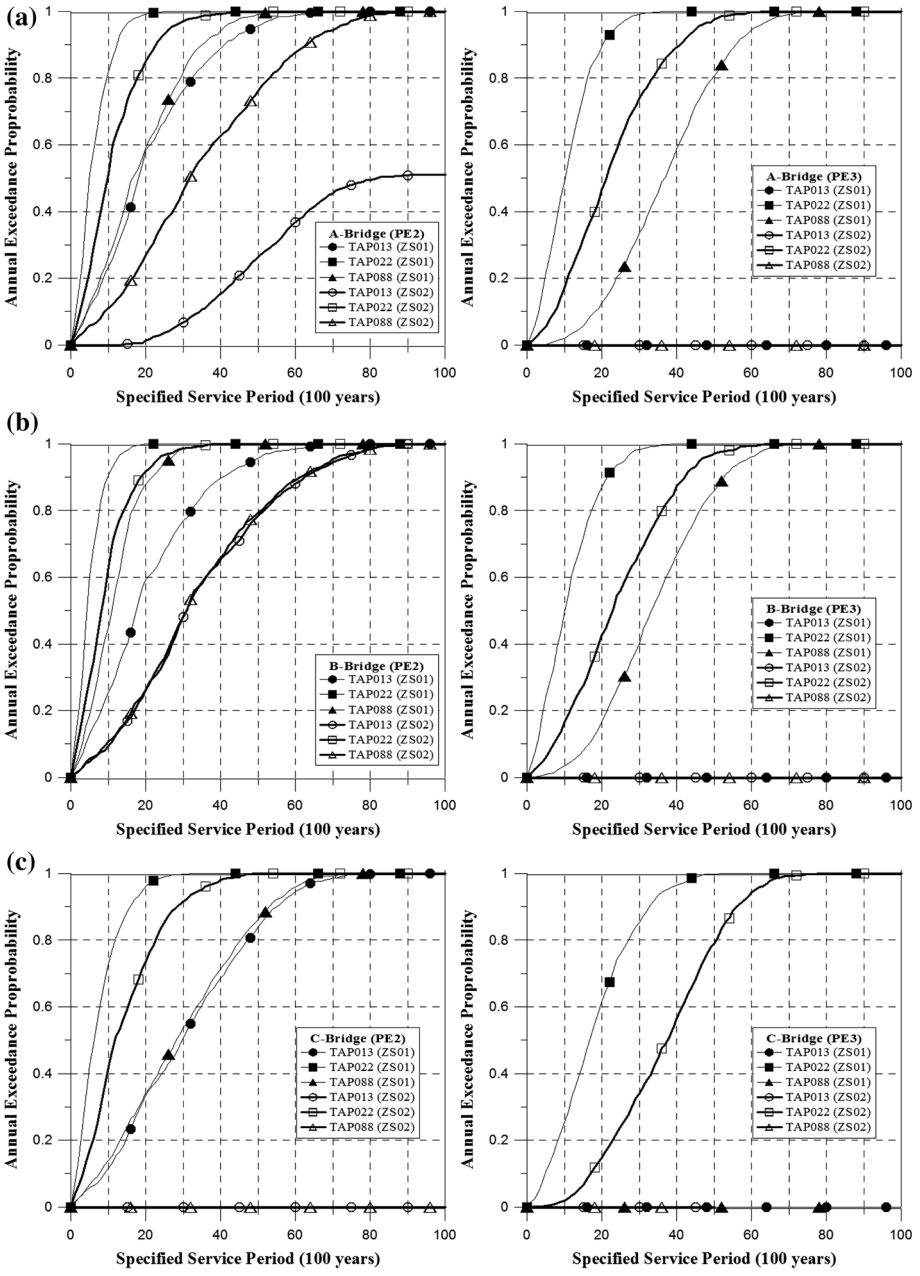


**Fig. 12** Exceedance probabilities of the specified damage states for the selected RC bridges. **a** Bridge-A, **b** Bridge-B, **c** Bridge-C

lives of Bridge-A, Bridge-B, and Bridge-C related to serviceability are 8, 10, and 12 years, respectively, when considering hypocenter ZS02; additionally, for hypocenter ZS01, their serviceability-related lives are roughly 4, 5, and 7 years, respectively. Clearly, when

estimating reliability-based service lives for the RC bridges while considering hypocenter ZS01, the difference in service lives for these three bridges is small.

### 5.2 Suao as an example: RC bridges with deterioration

For Bridge-A and Bridge-B, this work adopted their deterioration curves of structural performance from the literature (2011; Tables 5, 6). According to the deterioration curves of the structural performance for the RC bridges and the chloride-induced corrosion model (Sect. 2), the interpolation method was applied to derive the reduction coefficients of structural performance for the RC bridges within 100 years.

Figure 13 lists exceedance probabilities of specified damage states for the various settings of the selected RC bridges (0.1, 0.3, 1.0, and 3.0 km from the nearest coastline). Taking Bridge-B in Suao (ILA007) as an example, the exceedance probabilities of moderate damage state when considering hypocenter ZS01 are similar regardless of the distance between bridge location and the coastline of Suao; in other words, for the serviceability-related service life (Sect. 5.1), the effect of chloride-induced deterioration on exceedance probability of the moderate damage state can be neglected. However, for Bridge-A, the effect of chloride-induced deterioration on the serviceability-related and serviceability-related service lives cannot be neglected.

Tables 7 and 8 show the serviceability-related and safety-related service lives of the Bridge-A and Bridge-B considering the same reliability level stated in Sect. 5.2. Obviously, when the distance between the bridge's locations with the nearest coastline of Suao is longer than 1.0 km, the effect of the chloride-induced deterioration and cumulative seismic damage can be neglected in the estimation of the safety-related service life. Briefly, for deteriorating RC bridges, the proposed probability-based damage assessment method provides useful information related to maintenance based on both serviceability and safety.

**Table 5** Deterioration curves for the Bridge-A

| Distance to the nearest coastline (km) | Weight loss (%) | Reduction factor of $F_y$ | Reduction factor of $\delta_y$ | Reduction factor of $\delta_u$ |
|---|---|---|---|---|
| 0.1 | 33 | 0.31 | 0.29 | 0.42 |
| 0.3 | 19 | 0.31 | 0.33 | 0.42 |
| 1.0 | 7.0 | 0.77 | 0.77 | 0.70 |
| 3.0 | 2.0 | 0.92 | 0.94 | 0.88 |

**Table 6** Deterioration curves for the Bridge-B

| Distance to the nearest coastline (km) | Weight loss (%) | Reduction factor of $F_y$ | Reduction factor of $\delta_y$ | Reduction factor of $\delta_u$ |
|---|---|---|---|---|
| 0.1 | 28 | 0.31 | 0.31 | 0.63 |
| 0.3 | 16 | 0.46 | 0.48 | 0.75 |
| 1.0 | 6.0 | 0.90 | 0.91 | 0.78 |
| 3.0 | 2.0 | 0.97 | 1.00 | 1.00 |

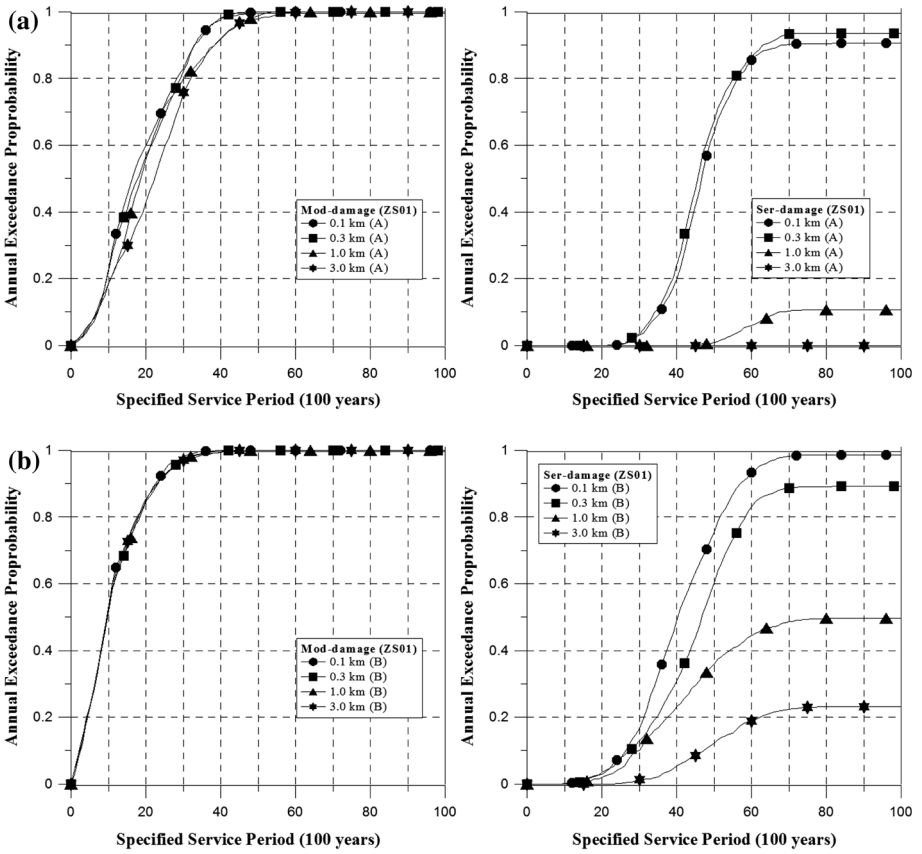


**Fig. 13** Exceedance probabilities of the specified damage states for the selected RC bridges considering various setting locations. **a** Bridge-A, **b** Bridge-B

**Table 7** Serviceability-related service life (years)

| Distance to the nearest coastline (km) | Bridge-A | Bridge-B |
|---|---|---|
| 0.1 | 15 | 10 |
| 0.3 | 17 | 10 |
| 1.0 | 18 | 10 |
| 3.0 | 23 | 10 |

**Table 8** Safety-related service life (years)

| Distance to the nearest coastline (km) | Bridge-A | Bridge-B |
|---|---|---|
| 0.1 | 45 | 40 |
| 0.3 | 47 | 47 |
| 1.0 | >100 | >100 |
| 3.0 | >100 | >100 |

## 6 Conclusions

This work analyzes probability-based damage states of unmaintained RC bridges while considering cumulative damage caused by earthquakes and chloride-induced deterioration using an integral simulation method. The proposed assessment procedure uses the concepts of life-cycle earthquake events and the seismic structural damage index to estimate occurrence probability of a specified damage state. Additionally, we assume the time at which earthquakes occur follows a Poisson process when analyzing seismic structural damage within a specified service period for a deteriorating RC bridge. Via reliable functions of serviceability- and safety-related service lives, an owner of, or investor in, an RC bridge can determine the effect of cumulative damage on maintenance planning. That is, one must consider this information when creating maintenance strategies. Restated, the proposed assessment procedure can help engineers understand whether the deterioration would accelerate the declining seismic performance of bridges and shorten their serviceability-related and safety-related service lives, as well as provide reference for repairing RC bridges and retrofitting their seismic performance. In the future, by combining the proposed method with LCC analysis for an RC bridge, seismic hazards and deterioration caused by carbonation or chloride ions can be considered when developing maintenance strategies.

**Acknowledgments** The authors would like to thank the National Science Council of the Republic of China, Taiwan, for financially supporting this research under Contract No. NSC100-2628-E-011-006.

## References

AIJ (1997) Recommendations for practice of survey, diagnosis and repair for deterioration of reinforced concrete structures. Architectural Institute of Japan, Tokyo (in Japanese)

ASTM C876 (1991) Standard test method for half-cell potential of uncoated reinforcing steel in concrete, American Society for Testing and Material

ATC (1996) Seismic evaluation and retrofit of concrete buildings. ATC-40 report, Applied Technology Council, Redwood City, California, USA

Chen YS, Chan YW (2010) On the correlation between air-borne chloride and durability of concrete in coastal region of north Taiwan, Master Thesis, National Taiwan University

Chiu CK, Noguchi T, Kanematsu M (2008) Optimal maintenance plan for RC members by minimizing life-cycle cost including deterioration risk due to carbonation. J Adv Concr Technol 6(3):469–480

Chiu CK, Jean WY, Chuang YT (2013) Optimal design base shear forces for reinforced concrete buildings considering seismic reliability and life-cycle costs. J Chin Inst Eng 36(4):458–470

CNS 13754 (1996) Standard test method for corrosion of metals and alloys-corrosivity of atmospheres-measurement of pollution. Bureau of Standards, Metrology & Inspection, Ministry of Economic Affairs of Taiwan, Taipei

CNS 13753 (2005) Standard test method for corrosion of metals and alloys-corrosivity of atmospheres-determination of corrosion rate of standard specimens for the evaluation of corrosivity. Bureau of Standards, Metrology & Inspection, Ministry of Economic Affairs of Taiwan, Taipei

Cosenza E, Manfredi G, Polese M (2009) Simplified method to include cumulative damage in the seismic response of single-degree-of-freedom systems. J Eng Mech (ASCE) 135(10):1081–1088

Das S, Gupta VK, Srimahavishnu V (2007) Damage-based design with no repairs for multiple events and its sensitivity to seismicity model. Earthq Eng Struct Dyn 36(3):307–325

Frangopol DM, Liu M (2007) Maintenance and management of civil infrastructure based on condition, safety, optimization, and life-cycle cost. Struct Infrastruct Eng 3(1):29–41

Izawa J, Matusima M (2004) The corrosion quantity of concrete crack induced by corrosion expansion, Master Thesis, Kagawa University

JSCE (2008) Reliability-based design for concrete structures (336 committee report), Tokyo: Japan Society of Civil Engineers

Jean WY, Chang YW, Wen KL, Loh CH (2002) Site Effects in the Taipei basin. Struct Eng 17(3):3–17
Kato Y, Uomoto T (2005) Proposal for quantitative evaluation methodology of inspection value in maintenance of concrete structures based on repair-risk. J Adv Concr Technol 3(3):363–370
Kong JS, Frangopol DM (2003) Life-cycle reliability-based maintenance cost optimization of deteriorating structures with emphasis on bridges. J Struct Eng 129(6):818–828
Kumar R, Gardoni P, Sanchez-Silva M (2009) Effect of cumulative seismic damage and corrosion on the life-cycle cost of reinforced concrete bridges. Earthq Eng Struct Dyn 38:887–905
MOTC (2010a) Environmental corrosivity classification for structures (1/2). Ministry of Transportation and Communications of Taiwan, Taipei
MOTC (2010b) Development of a bridge blockage detection and analysis model. Ministry of Transportation and Communications of Taiwan, Taipei
MOTC (2011) Environmental corrosivity classification for structures (2/2). Ministry of Transportation and Communications of Taiwan, Taipei
NCREE (2005) Estimation of maximum potential earthquakes and the shake map of ground motion. National Center for Research on Earthquake Engineering of Taiwan, Taipei
Niu DT (2003) Durability and life forecast of reinforced concrete structure. Science press, Beijing (in Chinese)
Padgett JE, Dennemann K, Ghosh J (2010) Risk-based seismic life-cycle cost-benefit (LCC-B) analysis for bridge retrofit assessment. Struct Saf 32:165–173
Park YJ, Ang AH-S (1985) Mechanistic seismic damage model for reinforced concrete. J Struct Eng 111(4):722–739
Sanchez-Silva M, Klutke GA, Rosowsky DV (2011) Life-cycle performance of structures subject to multiple deterioration mechanisms. Struct Saf 33(3):206–217
Sung YC, Huang CH, Liu KY, Wang CH, Su CK, Chang KC (2010) Life-cycle evaluation of deteriorated structural performance of neutralized reinforced concrete bridges. Struct Infrastruct 6(6):741–751
Suzuki M, Ibayashi K, Fujiwara M, Ozaka Y (1998) Relevance of earthquake ground motion and structural characteristics to damage of reinforced concrete pier. J Struct Eng 44A:651–658
Takahashi Y, Der Kiureghian A, Ang AH-S (2004) Life-cycle cost analysis based on a renewal model of earthquake occurrences. Earthq Eng Struct Dyn 33(7):859–880
Takahashi T, Sakai M, Seki H, Matsushima M (2005) Calculation of LCC and selection system of repairing method for reinforced concrete members exposed to sea environments. Concr Res Technol 16(3):21–29 (in Japanese)
Takahashi N, Nakano Y, Shiohara H (2006) Reparability demand spectrum of R/C buildings due to the lifecycle seismic loss estimation. First European Conference on Earthquake Engineering and Seismology (1st ECEES), Geneva, Switzerland
Takeda T, Sozen MA, Nilson NN (1972) Reinforced concrete response to simulated earthquake. J Struct Eng 96(12):2557–2573
Tottori S, Miyagawa T (2004) Deterioration prediction of concrete structures concerning rebar corrosion due to carbonation. Proceedings of Japan Society of Civil Engineers (JSCE), 767:35–46
Williams RJ, Gardoni P, Bracci JM (2009) Decision analysis for seismic retrofit of structures. Struct Saf 31:188–196